ISSN 1063-7834, Physics of the Solid State, 2009, Vol. 51, No. 9, pp. 1800–1808. © Pleiades Publishing, Ltd., 2009.
Original Russian Text © Yu.V. Zorenko, V.I. Gorbenko, 2009, published in Fizika Tverdogo Tela, 2009, Vol. 51, No. 9, pp. 1697–1704.

SEMICONDUCTORS AND DIELECTRICS

Growth and Luminescence Properties of Perovskite Single-Crystalline Films $R\mathrm{AlO_3}$ (R = Lu, Lu–Y, Y, Tb)

Yu. V. Zorenko* and V. I. Gorbenko

Franko National University of L'viv, Universitetskaya ul. 1, Lviv, 79000 Ukraine

** e-mail: zorenko@elektronics.wups.lviv.ua*

Received November 26, 2008; in final form, January 12, 2009

Abstract—The conditions and the mechanisms of crystallization of undoped and Ce^{3+}-doped single-crystalline films $R\mathrm{AlO_3}$ (R = Lu, Lu–Y, Y, Tb) by liquid-phase epitaxy on $\mathrm{YAlO_3}$ single-crystalline substrates at a considerable mismatch between the lattice constants of the single-crystalline films and the substrate are analyzed. The maximum values of this mismatch at which the stable growth of the single-crystalline films is observed are determined. It is demonstrated that there are transition layers between the substrate and the grown single-crystalline film in which the difference between the lattice parameters of the single-crystalline film and the substrate level off. The optical and luminescence characteristics of the undoped and Ce^{3+}-doped single-crystalline films $R\mathrm{AlO_3}$ (R = Y, Y–Lu, Lu, Tb), as well as the scintillation characteristics of the (Lu–Y)$\mathrm{AlO_3}$: Ce single-crystalline films upon excitation by alpha particles of the ^{239}Pu source (5.15 MeV), are investigated.

PACS numbers: 78.55.Hx, 78.47.+p, 71.55.Ht

DOI: 10.1134/S1063783409090078

1. INTRODUCTION

In recent two decades, apart from a wide use in bubble memory and other magneto-optical devices [1], rare-earth and yttrium oxide single-crystalline films have found extensive application as thin-film laser media [2, 3], scintillators for the radiation monitoring of alpha and beta particles [4, 5], cathodoluminescence screens [6, 7], and screens for visualization of X-ray images with a high spatial resolution [8, 9]. The single-crystalline films based on compounds with a garnet structure, primarily, the $\mathrm{Y_3Al_5O_{12}}$ single-crystalline films doped with rare-earth ions (Ce^{3+}, Pr^{3+}, Tb^{3+}, Nd^{3+}, Yb^{3+}) and transition metal ions (Cr^{3+}, Mn^{3+}) [2–10], as well as the rare-earth garnet single-crystalline films, in particular, $\mathrm{Lu_3Al_5O_{12}}$ [4–10] and $\mathrm{Tb_3Al_5O_{12}}$ [11, 12] single-crystalline films, have been predominantly used in the majority of the above applications.

As a rule, rare-earth garnet single-crystalline films have been prepared using liquid-phase epitaxy from melt solutions based on a $\mathrm{PbO–B_2O_3}$ flux on substrates from a considerably cheaper garnet, for example, $\mathrm{Y_3Al_5O_{12}}$ [10–12]. It should be noted that the specific feature of crystallization of the $\mathrm{Lu_3Al_5O_{12}}$ and $\mathrm{Tb_3Al_5O_{12}}$ single-crystalline films on the $\mathrm{Y_3Al_5O_{12}}$ substrates is a large difference Δa between the lattice parameters of the single-crystalline film and the substrate [9, 12]. In our earlier work [12], we established the limiting values of this quantity $+0.1\ \text{Å} > \Delta a > -0.094\ \text{Å}$ at which the stable growth of qualitative single-crystalline films of the $R_3\mathrm{Al_5O_{12}}$ (R = Lu, Yb, Tb, Y–Eu) garnets on the $\mathrm{Y_3Al_5O_{12}}$ substrates is possible without any additional doping with the aim of decreasing the difference Δa.

Unlike the crystallization of garnet single-crystalline films, information on the conditions for the crystallization of single-crystalline films of one more widely used class of oxide compounds, i.e., perovskites, by liquid-phase epitaxy is considerably scarcer. It should be noted that perovskite single-crystalline films offer a number of advantages over their analogs based on garnet single-crystalline films. First and foremost, these advantages lie in higher densities and larger X-ray absorption coefficients for perovskite single-crystalline films as compared to garnet single-crystalline films [9, 13], as well as the possibility of achieving a higher luminescence efficiency for Ce^{3+} and Pr^{3+} ions due to the shift of the emission spectrum of these ions toward the UV range and decreasing their luminescence decay time [14].

In 1999, we prepared the first undoped and Ce^{3+}-doped $\mathrm{YAlO_3}$ single-crystalline films on substrates consisting of this perovskite [15]. At approximately the same time, Ferrand et al. [16] reported on the crystallization of $\mathrm{YAlO_3}$ single-crystalline films doped with rare-earth ions that can be used as laser media. More recently (in 2005), we first crystallized undoped and Ce^{3+}-doped $\mathrm{LuAlO_3}$ single-crystalline films on $\mathrm{YAlO_3}$ substrates without any additional doping in order to match the lattice parameters of the single-crystalline film and the substrate [17]. However, the general reg-

Table 1. Lattice constants of some perovskites, as well as absolute and relative values of the lattice constant mismatches Δa, Δb, and Δc, in the growth of the perovskite single-crystalline films on the undoped $YAlO_3$ single-crystalline substrates

Composition of the single-crystalline film	a, Å	Δa, Å (Δa, %)	b, Å	Δb, Å (Δb, %)	c, Å	Δc, Å (Δc, %)
$YAlO_3$	5.18004	–	5.30842	–	7.36301	–
$TbAlO_3$	5.22961	+0.04957 (+0.957)	5.30692	−0.0015 (−0.028)	7.41543	0.05243 (+0.71)
$LuAlO_3$	5.10564	−0.0744 (−1.436)	5.33417	+0.02575 (+0.484)	7.30532	−0.05747 (−0.743)

Table 2. Growth conditions for the (Y–Lu)AlO_3 single-crystalline films on the $YAlO_3$ substrates

Parameter	$LuAlO_3$: Ce	$Y_{0.2}Lu_{0.8}AlO_3$: Ce	$Y_{0.4}Lu_{0.6}AlO_3$: Ce	$YAlO_3$: Ce	$TbAlO_3$: Ce
$R_1 = [PbO]/[B_2O_3]$	11.74	11.74	11.74	11.85–11.6	12.0
$R_2 = [Y_2O_3(Lu_2O_3)]/[Al_2O_3]$	1.0	1.0	1.0	1.0	1.0
$R_3 = \Sigma R_2O_3/[PbO + B_2O_3]$	0.0335	0.04	0.0503	0.026–0.02	0.0356
$R_4 = [CeO_2]/[\Sigma R_2O_3]$	0.2	0.165	0.129	0.1–0.17	0.1–0.19
Growth temperature T_g, °C	980–1020	1000–1040	1030–1070	960–1000	950–970
Substrate rotation rate ω in the melt solution, rpm	100	100	100	100	100
Growth rate f of the single-crystalline film, μm/min	0.35–0.7	1–1.2	0.4–0.7	0.17–1.3	0.3–1.08
Thickness of the single-crystalline film, μm	7–21	12–24	8–13	7–57	7.0–40

ularities of crystallization of rare-earth perovskite single-crystalline films have not been analyzed and the limiting conditions for their growth on the $YAlO_3$ substrates have not been revealed to date.

The purpose of this work was to establish these conditions and the mechanism of crystallization of rare-earth perovskite single-crystalline films by using the growth of single-crystalline films $RAlO_3$ (R = Y, Y–Lu, Lu, Tb) on $YAlO_3$ substrates through liquid-phase epitaxy as an example. It should be noted that the data on the crystallization of the single-crystalline films based on the $TbAlO_3$ compounds are reported for the first time. The results obtained together with the data on the crystallization of the garnet single-crystalline films [12] are analyzed in order to reveal the general regularities and the conditions for the crystallization of single-crystalline films of oxides in the Y_2O_3–Al_2O_3–R_2O_3 system with different structure types.

2. SPECIFIC FEATURES OF THE GROWTH OF SINGLE-CRYSTALLINE FILMS $RALO_3$ (R = LU, LU–Y, Y, TB) ON $YALO_3$ SUBSTRATES

Undoped and Ce^{3+}-doped single-crystalline films $RAlO_3$ (R = Lu, Lu–Y, Y, Tb) on $YAlO_3$ single-crystalline substrates were grown by liquid-phase epitaxy in air from melt solutions based on a PbO–B_2O_3 flux and crystal-forming components R_2O_3 (R = Y, Lu, Tb) and Al_2O_3 at a considerable mismatch between the lattice parameters of the single-crystalline films and the substrate (Table 1). In the growth of the single-crystalline film based on the $TbAlO_3$ perovskite, the Tb_4O_7 oxide instead of the Tb_2O_3 oxide was used as the crystal-forming component. The thickness of the grown single-crystalline films was determined by the weight method. The growth of single-crystalline films of all the above compositions was characterized by a linear dependence of the crystallization rate of the single-crystalline films on the growth temperature T_g. The characteristics of the corresponding melt solutions and the conditions for the growth of the single-crystalline films are summarized in Table 2.

Figure 1 shows the experimentally determined fragment of the concentration triangle of the (Y_2O_3–Lu_2O_3)–((Y_2O_3–Lu_2O_3) + Al_2O_3)–(PbO–B_2O_3) pseudoternary system in the growth of $Lu_{1-x}Y_xAlO_3$ (x = 0–1) single-crystalline films. The mole fractions of the oxides in the batch are plotted along the axes. The closed squares correspond to the calculated compositions of the batch of the melt solutions from which the (Y–Lu)AlO_3 single-crystalline films were grown.

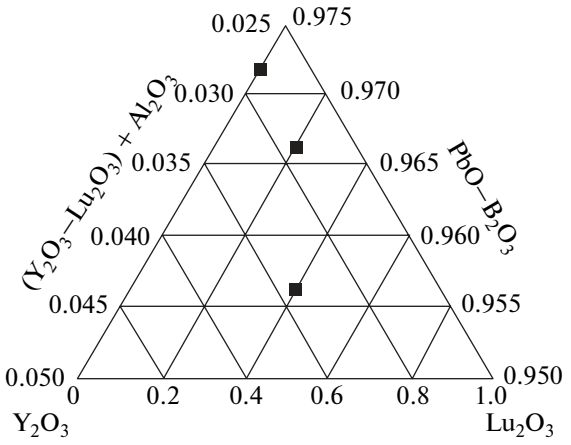

Fig. 1. Fragment of the concentration triangle of the $(Y_2O_3–Lu_2O_3)–\{(Y_2O_3–Lu_2O_3) + Al_2O_3\}–(PbO–B_2O_3)$ pseudoternary system in the growth of $Lu_{1-x}Y_xAlO_3$ ($x = 0–1$) single-crystalline films.

The X-ray microanalysis of the compositions of some samples of the $YAlO_3$: Ce and $LuAlO_3$: Ce single-crystalline films made it possible to determine the segregation coefficients of Ce^{3+} ions in the crystallization of these perovskites. In particular, in the growth of the single-crystalline films of the aforementioned compositions on the $YAlO_3$ substrates, the segregation coefficients of Ce^{3+} ions are equal to 0.010 and 0.002, respectively. The segregation coefficients of Ce^{3+} ions in the $Lu_{1-x}Y_xAlO_3$ ($x = 0–1$) solid solution single-crystalline films were similarly determined to be 0.0090 and 0.0043 at $x = 0.4$ and 0.2, respectively. Therefore, the incorporation coefficient of Ce^{3+} ions gradually decreases during the replacement of Y^{3+} cations by Lu^{3+} cations in the composition of the $Lu_{1-x}Y_xAlO_3$ single-crystalline films.

The experimentally determined lattice constants of the single-crystalline films of the perovskites under investigation and the mismatches Δa between the lattice constants of the single-crystalline films and the $YAlO_3$ substrate are listed in Table 1. It should be noted that, in the growth of the $RAlO_3$ (R = Lu, Lu–Y, Tb) single-crystalline films, we did not use any additional doping in order to decrease the difference between the lattice constants of the single-crystalline films and the substrate. However, the possibility of crystallizing the $RAlO_3$ (R = Lu, Lu–Y, Tb) single-crystalline films on the $YAlO_3$ substrates was demonstrated and the growth conditions of these single-crystalline films with a good structural and optical quality were chosen for the first time.

It should be specially noted that, apart from the aforementioned works, no data on the crystallization of rare-earth perovskite single-crystalline films by liquid-phase epitaxy are available in the literature. Therefore, we can argue that the results of the study of crystallization of the $RAlO_3$ (R = Lu, Lu–Y, Tb) single-crystalline films allowed us to determine the limiting values of the mismatch between the lattice parameters of the single-crystalline films and the $YAlO_3$ substrate at which the stable growth of the single-crystalline films of the above compositions (Table 1) is possible. It should be noted that the revealed limiting conditions for the growth of the single-crystalline films of these perovskites (Table 1) appear to be even wider as compared to the limiting conditions determined in our previous work [12] for the absolute and relative values of the mismatch between the lattice constants of the single-crystalline films and the substrate – 0.93 Å $\le \Delta a \le$ 0.1 Å (–0.775% $\le \Delta a \le$ +0.833%) in the growth of the single-crystalline films of the $R_3Al_5O_{12}$ (R = Y–Eu, Tb, Lu) garnets by liquid-phase epitaxy on the $Y_3Al_5O_{12}$ single-crystalline substrates. This makes it possible to extend significantly a possible class of functional devices based on garnet and perovskite single-crystalline films crystallized by liquid-phase epitaxy on relatively cheaper and more available $Y_3Al_5O_{12}$ and $YAlO_3$ substrates.

The nontrivial fact that single-crystalline films of the $RAlO_3$ (R = Y, Lu, Tb) rare-earth perovskites can be crystallized on the $YAlO_3$ substrates for such a considerable mismatch between the lattice constants of the single-crystalline films and the substrate requires a detailed explanation. We believe that one of the possible mechanisms of leveling of this large difference between the lattice constants of the substrate and the single-crystalline films is the formation of transition layers (TLs) at the single-crystalline film–substrate interface. The formation of the transition layers 0.1–0.5 μm in thickness was observed by Telesnin et al. [18] in the crystallization of single-crystalline films based on the $Y_3Fe_5O_{12}$ compound by liquid-phase epitaxy on $Gd_3Gd_5O_{12}$ single-crystalline substrates. The formation of these transition layers and their structure in the crystallization of the single-crystalline films of the $R_3Al_5O_{12}$ (R = Lu, Tb, Eu–Y) garnets by liquid-phase epitaxy on the $Y_3Al_5O_{12}$ substrates were investigated in more detail in our earlier works [11, 12]. It was revealed that the formation of the transition layers in the form of the $(R–Y)_3Al_5O_{12}$ solid solution is the main mechanism that favors the crystallization of the $R_3Al_5O_{12}$ (R = Lu, Tb, Eu–Y) garnet single-crystalline films by liquid-phase epitaxy on the $Y_3Al_5O_{12}$ substrates at large mismatches between the lattice parameters of the single-crystalline films and the substrate: $\Delta a \le \pm 1.0$ Å [12].

In order to confirm the formation of the transition layers in the crystallization of the perovskite single-crystalline films on the $YAlO_3$ substrates, we obtained the cathodoluminescence images of the single-crystalline film–substrate interface in cleavages of the epitaxial structures consisting of the $TbAlO_3$: Ce (Figs. 2c, 2d) or $LuAlO_3$: Ce (Figs. 2e, 2f) single-crystalline

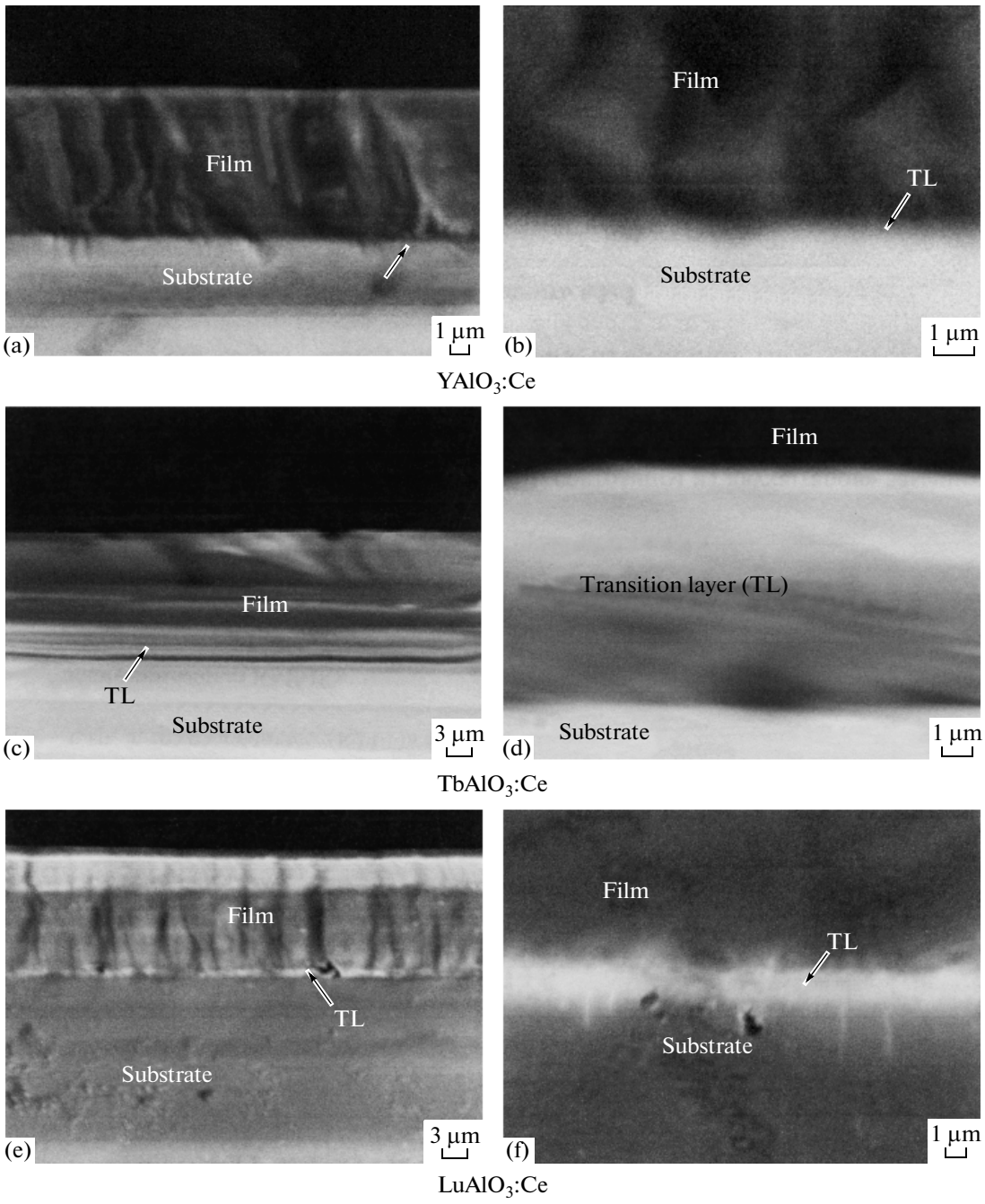

Fig. 2. Cathodoluminescence images of the transition layers (at the center) between the $YAlO_3$ substrates (at the bottom) and the single-crystalline films (at the top) at different magnifications in the crystallization of the (a, b) $YAlO_3$: Ce, (c, d) $TbAlO_3$: Ce, and (e, f) $LuAlO_3$: Ce single-crystalline films 22, 8.8, and 21 μm in thickness, respectively.

films and the $YAlO_3$ substrates and compared them with the corresponding images of the interface in the cleavage of the homoepitaxial structure consisting of the $YAlO_3$ single-crystalline film grown on the $YAlO_3$ substrate (Figs. 2a, 2b). It can be clearly seen from the cathodoluminescence images of the single-crystalline film–substrate interface that these transition layers with a thickness of several hundreds of nanometers are formed even in the homoepitaxial crystallization of the $YAlO_3$ single-crystalline film (Figs. 2a, 2b). The transition layer thickness increases considerably to 1–3 μm in the crystallization of the $TbAlO_3$: Ce (Figs. 2c, 2d) and $LuAlO_3$: Ce (Figs. 2e, 2f) single-crystalline films on the $YAlO_3$ substrates.

As in the case of the crystallization of the garnet single-crystalline films [12], we can assume that the composition of the transition layers in the growth of

Table 3. Comparison of light yields for the single crystals and single-crystalline films of the (Lu–Y)AlO_3 : Ce perovskites upon excitation by α particles of the ^{239}Pu source (5.15 MeV)

Perovskite	Relative light yield*, %
$LuAlO_3$: Ce single-crystalline film	2.7
$Lu_{0.8}Y_{0.2}AlO_3$: Ce single-crystalline film	3.7
$Lu_{0.6}Y_{0.4}AlO_3$: Ce single-crystalline film	13.4
$YAlO_3$: Ce single-crystalline film	32.7
$Lu_{0.3}Y_{0.7}AlO_3$: Ce single crystal	60.8
$YAlO_3$: Ce single crystal	100

* For the FEU-100 (λ_{max} = 250–375 nm).

the single-crystalline films of the $RAlO_3$ (R = Lu, Tb) perovskites can be described by the formula $R_xY_{1-x}AlO_3$ (x = 0–1). We believe that, the initial stage of the growth of the single-crystalline films involves the formation of the $YAlO_3$ epitaxial sublayer homogeneous with respect to the substrate composition. The Y^{3+} ions in a small amount are contained in the melt solution due to the partial dissolution of the surface of the $YAlO_3$ substrate at the initial stage of the epitaxial growth. Then, a part of Y^{3+} cations in this sublayer is replaced by Lu^{3+} or Tb^{3+} cations. This results in the step-by-step formation of the transition layer in the form of the $R_xY_{1-x}AlO_3$ (x = 0–1) solid solution with the required composition, which is completed by the onset of crystallization of the main bulk of the $RAlO_3$ (R = Lu, Lu–Y, Tb) single-crystalline film. It should be noted that a specific role in a decrease in the lattice constant mismatch can be played by the incorporation of Pb^{2+} trace impurity ions (with a larger ionic radius as compared to the ionic radii of the main cations) into the composition of the transition layer.

3. OPTICAL, LUMINESCENCE, AND SCINTILLATION PROPERTIES OF SINGLE-CRYSTALLINE FILMS $RALO_3$ (R = LU, LU–Y, Y, TB)

Investigations into the optical, luminescence, and scintillation properties of the perovskite single-crystalline films involved the measurements of the absorption and cathodoluminescence spectra and the light yield of the radioluminescence upon excitation with alpha particles of a ^{239}Pu source (5.15 MeV). The absorption spectra were recorded on a Specord M40 UV-VIS spectrophotometer at a temperature of 300 K. The cathodoluminescence spectra were measured on an automated setup based on an SF-4A monochromator and an FÉU-100 photomultiplier upon excitation of the samples with an electron beam (10 kV, 5 μa) at temperatures of 300 and 80 K with a correction for the spectral sensitivity of the detection channel. Some emission spectra of the single-crystalline films at a temperature of 10 K and the decay kinetics of Ce^{3+} luminescence at a temperature of 300 K were measured upon excitation with pulsed synchrotron radiation (pulse duration, 0.126 ns; repetition time, 200 ns) on the Superlumi station at the HASYLAB (DESY, Hamburg, Germany). The light yield of the radioluminescence of the single-crystalline films was measured in a scintillation detector based on the FÉU-100 photomultiplier upon excitation with alpha particles of the ^{239}Pu source (5.15 MeV). In this case, the single-crystalline film samples and the radiation sources were located directly on the exit window of the photomultiplier.

3.1. Single-crystalline Films Based on (Y,Lu)AlO_3 and (Y,Lu)AlO_3 : Ce Perovskites

The absorption spectra of the $YAlO_3$ and $YAlO_3$: Ce single-crystalline films (4 and 332 μm in thickness, respectively) grown on the $YAlO_3$ substrates are shown in Fig. 3a (curves *1*, *2*). For comparison, the absorption spectrum of the $YAlO_3$: Ce single crystal is also depicted in Fig. 3 (curve *3*). The broad triplet absorption band with maxima at 275, 291, and 303 nm corresponds to the $4f^1\,(^2F_{5/2}) \longrightarrow 5d\,(^2T_{2g})$ transitions in the Ce^{3+} ions. The other two bands located at 219 and 238 nm are associated with the $4f^1\,(F_{5/2}) \longrightarrow 5d\,(^2E)$ transitions in these ions. The spectra of the single-crystalline films also contain intense absorption bands at 230 and 210 nm, which are attributed to the $^1S_0 \longrightarrow {}^3P_1$ intracenter transitions with the charge transfer $Pb^{2+} \longrightarrow Pb^{3+} + e$ in the Pb^{2+} ion trace impurity that dopes the single-crystalline films in their crystallization from the lead-containing melt solutions. It can be seen from Fig. 3a that, unlike the $YAlO_3$: Ce single crystal, the absorption bands of the Ce^{3+} ions in the range 220–240 nm in the spectra of the single-crystalline films overlap considerably with the intense absorption in this range due to the presence of the Pb^{2+} ions.

Figure 3b shows the absorption spectra of the $LuAlO_3$: Ce (curve *1*) and $Lu_{1-x}Y_xAlO_3$: Ce (x = 0.2, 0.4) (curves *2*, *3*) single-crystalline films in comparison with the absorption spectrum of the $Lu_{0.3}Y_{0.7}AlO_3$: Ce single crystal (curve *4*). The spectra of these single-crystalline films also involve the intense absorption bands of the Pb^{2+} ions in the range 200–230 nm. This absorption decreases with an increase in the content of Y^{3+} ions in the composition of the single-crystalline films (Fig. 3b, curves 2, 3), which, in turn, leads to an increase in the light yield for these single-crystalline films (Table 3). The increase in the light yield is associated not only with the increase in the content of Y^{3+} ions and the decrease in the concentration of the Pb^{2+} trace impurity in the composition of the single-crystalline films but also with the increase in the incorporation coeffi-

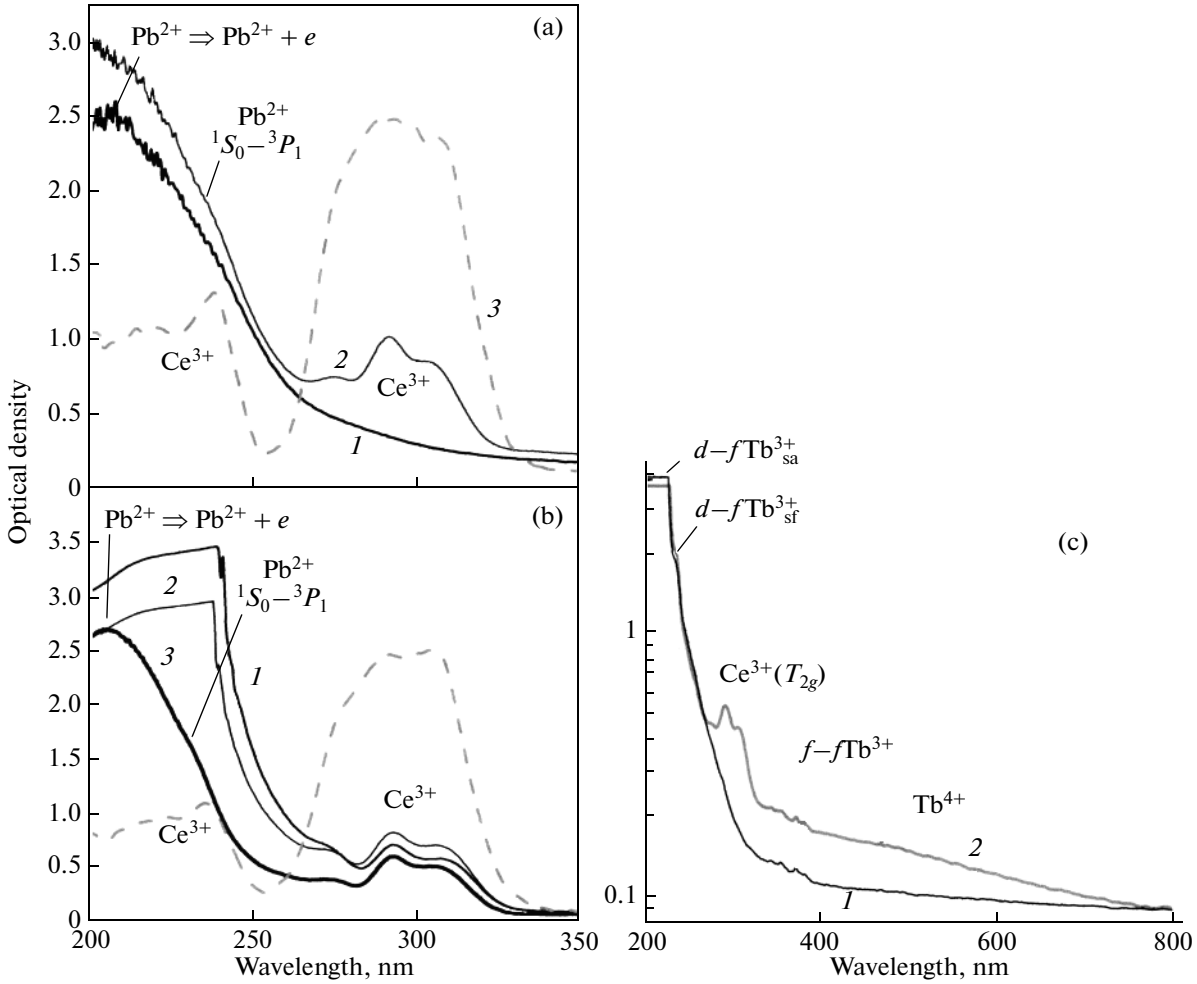

Fig. 3. (a) Absorption spectra of the (*1*) $YAlO_3$ and (*2*) $YAlO_3$: Ce single-crystalline films (4 and 33 μm in thickness, respectively) in comparison with (*3*) the absorption spectrum of the $YAlO_3$: Ce single crystal 1 mm in thickness. (b) Absorption spectra of the (*1*) $LuAlO_3$: Ce (20 mol % CeO_2 in the melt solution), (*2*) $Lu_{0.8}Y_{0.2}AlO_3$: Ce (16.6 mol % CeO_2 in the melt solution), and (*3*) $Lu_{0.6}Y_{0.4}AlO_3$: Ce (12.9 mol % CeO_2 in the melt solution) single-crystalline films (21.0, 25.0, and 12.6 μm in thickness, respectively) in comparison with (*4*) the absorption spectrum of the $Lu_{0.3}Y_{0.7}AlO_3$: Ce single crystal 1 mm in thickness. (c) Absorption spectra of the (*1*) $TbAlO_3$ and (*2*) $TbAlO_3$: Ce single-crystalline films (9.0 and 8.8 μm in thickness, respectively). All single-crystalline films were prepared by liquid-phase epitaxy on the $YAlO_3$ substrates 0.5 mm in thickness.

cient of Ce^{3+} ions in the growth of the $Lu_{1-x}Y_xAlO_3$: Ce single-crystalline films as compared to the crystallization of the $LuAlO_3$: Ce single-crystalline film. This circumstance can be explained by the difference between the ionic radii of the Lu^{3+} (1.19 Å), Y^{3+} (1.22 Å), Tb^{3+} (1.25 Å), Ce^{3+} (1.34 Å), and Pb^{2+} (1.49 Å) ions occupying cubo-octahedral sites in the perovskite lattice [19]. In the growth of the $LuAlO_3$ single-crystalline films on the $YAlO_3$ substrates, the difference between the ionic radii of the cations in the cubo-octahedral sites of the single-crystalline film and substrate is equal to 0.03 Å. This favors the incorporation of large-sized ions (Pb^{2+}) into the composition of the grown single-crystalline films, whereas the replacement of a part of Lu^{3+} ions by Y^{3+} ions decreases this difference and increases the probability of incorporation of small-sized ions (Ce^{3+}). Nonetheless, the last process does not completely exclude the incorporation of Pb^{2+} ions into the composition of the single-crystalline films and only decreases their concentration.

In view of the presence of lead ions and their quenching effect on the Ce^{3+} luminescence, the $LuAlO_3$: Ce and $YAlO_3$: Ce single-crystalline films are characterized by a significantly lower light yield of the radioluminescence upon excitation by alpha particles of the ^{239}Pu source (5.15 MeV). The corresponding yields amount to ~4.5 and 32.7% of the light yields for their single-crystalline analogs, respectively (Table 3). The doping of the $Lu_{1-x}Y_xAlO_3$: Ce single-crystalline films with Y^{3+} ions makes it possible to decrease the content of the trace impurity of Pb^{2+} ions and to increase the concentration of Ce^{3+} ions. This results in

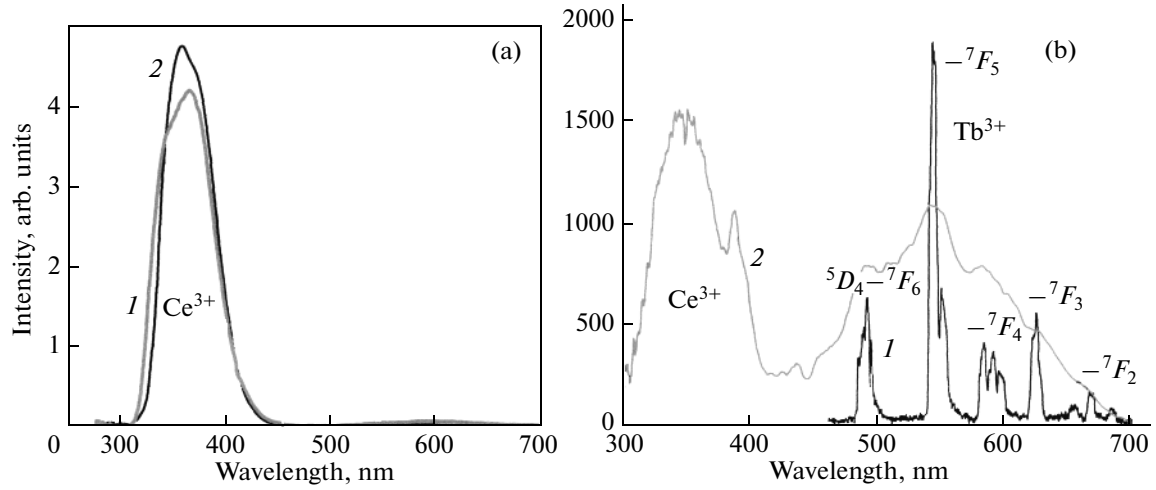

Fig. 4. (a) Cathodoluminescence spectra of the (*1*) $YAlO_3$: Ce and $LuAlO_3$: Ce single-crystalline films at a temperature of 300 K. (b) Luminescence spectra of the (*1*) $TbAlO_3$ and (*2*) $TbAlO_3$: Ce single-crystalline films at a temperature of 10 K upon excitation by synchrotron radiation with a wavelength of 166 nm.

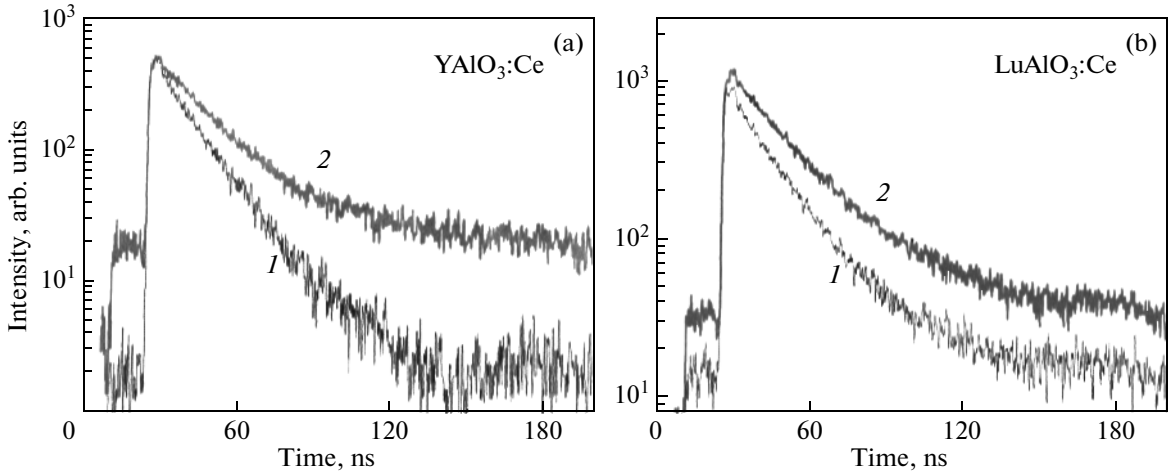

Fig. 5. Decay kinetics of Ce^{3+} luminescence for (a) the $YAlO_3$: Ce single-crystalline film at $\lambda = 375$ nm and (b) the $LuAlO_3$: Ce single-crystalline film at $\lambda = 370$ nm upon excitation with synchrotron radiation (*1*) in the range of the 4*f*–5*d* transitions of the Ce^{3+} ions with a wavelength of 295 nm and (*2*) in the range of the interband transitions with a wavelength of 145–160 nm at a temperature of 300 K.

a somewhat increase in the light yield to 22% of the light yield for the corresponding bulk single crystal in the series of $Lu_{1-x}Y_xAlO_3$: Ce single-crystalline films with an increase in the content x in the range 0–0.4 (Table 3).

Figure 4a shows the cathodoluminescence spectra of the Ce^{3+}-doped $YAlO_3$: Ce (curve *1*) and $LuAlO_3$: Ce single-crystalline films (curve *2*) prepared by liquid-phase epitaxy on the $YAlO_3$ substrates. The intense luminescence bands in the range 358–365 nm are associated with the $5d\,(^2T_{2g}) \longrightarrow 4f\,(^2F_{5/2,\,7/2})$ radiative transitions in the Ce^{3+} ions. The low-intensity luminescence bands in a range of 600 nm are attributed to the long-wavelength emission band of the trace impurity of Pb^{2+} ions as the flux component. On the whole, the luminescence spectra of the $YAlO_3$: Ce and $LuAlO_3$: Ce single-crystalline films (Fig. 4a, curves *1*, *2*) are identical to those of their bulk single-crystalline analogs [13].

Figure 5 shows the decay kinetics of the Ce^{3+} luminescence for the $YAlO_3$: Ce (Fig. 5a) and $LuAlO_3$: Ce (Fig. 5b) single-crystalline films upon intracenter and band–band excitations by pulsed synchrotron radiation with the wavelength $\lambda = 145$–160 nm in the range of interband transitions of these perovskites [17]. The decay times of the main emission component are $\tau =$ 13.9 and 22.4 ns for the $YAlO_3$: Ce single-crystalline film (Fig. 5a) and $\tau = 16.9$ and 23.3 ns for the $LuAlO_3$

: Ce single-crystalline film (Fig. 5b) in the case of the intracenter excitation (λ = 295 nm, curves *1*) and interband excitation (λ = 145–160 nm, curves *2*) of the Ce^{3+} luminescence (Fig. 5), respectively. It should be noted that the aforementioned decay times of the Ce^{+} luminescence upon excitation in the range of the interband transitions in the $YAlO_3$: Ce and $LuAlO_3$: Ce single-crystalline films are considerably shorter than those (28–32 ns) for the bulk single-crystalline analogs of these perovskites [13]. The reason is that the single-crystalline films do not contain antisite defects of the Y_{Al} and Lu_{Al} type (their concentration in the single crystals is as high as 1–2% of the total content of Y and Lu cations [20]) and that the concentration of vacancy-type defects, primarily, oxygen vacancies, is low due to the low growth temperature of the single-crystalline films in air.

3.2. $TbAlO_3$ and $TbAlO_3$: Ce Single-Crystalline Films

The absorption spectra of the $TbAlO_3$ and $TbAlO_3$: Ce single-crystalline films are depicted in Fig. 3c. In the range 330–390 nm, the absorption spectra of these single-crystalline films contain narrow bands with maxima at 342.0, 353.5, 371.0, and 380.5 nm due to the transitions from the $^7F_6$ level of the ground state to the $^5L_9$, $^5G_4$, $^5L_{10}$, and $^5G_6 + {}^5D_3$ terms of the 4*f* shell of the Tb^{3+} cations, respectively [21]. The absorption band at 485 nm corresponding to the $^7F_6 \longrightarrow {}^5D_4$ transition [21] is almost not observed due to the small thickness of the single-crystalline films. In the short-wavelength range, the absorption spectrum of the $TbAlO_3$ and $TbAlO_3$: Ce single-crystalline films contain a group of bands with maxima at 232 and 215 nm, which are attributed to the spin-allowed (sa) and spin-forbidden (sf) transitions 4*f*–5*d* in the Tb^{3+} ions [22]. The absorption bands associated with the other 4*f*–5*d* transitions of the Tb^{3+} cations are located in the range <200 nm (Fig. 3c).

Apart from the aforementioned absorption bands of the Tb^{3+} cations, the absorption spectra of the $TbAlO_3$: Ce single-crystalline film involve the triplet absorption band of the Ce^{3+} ions with maxima at 274, 290, and 305 nm, which is assigned to the $4f^1$ ($^2F_{5/2}$) $\longrightarrow$ 5*d* ($^2T_{2g}$) transitions in the Ce^{3+} ions. The other two bands attributed to the $4f^1$ ($^2F_{5/2}$) $\longrightarrow$ 5*d* (^2E) transitions in the Ce^{3+} ions overlap with the *d*–*f* absorption bands of the Tb^{3+} cations. It should be noted that the absorption spectra of the single-crystalline films based on the $TbAlO_3$ perovskite also involve the intense band with a maximum at 465 nm, which is most likely corresponds to the absorption of the Tb^{4+} ions [23]. The presence of cations in this charge state at some concentration in the single-crystalline films based on the $TbAlO_3$ perovskite is caused by the use of the Tb_4O_7 oxide as the initial material and the doping of the single-crystalline film with the Pb^{2+} trace impurity ions.

The luminescence spectrum of the $TbAlO_3$ single-crystalline film at a temperature of 10 K upon excitation by synchrotron radiation with a wavelength of 166 nm in the fundamental absorption range of this perovskite is depicted in Fig. 4b. The luminescence spectrum of the $TbAlO_3$ single-crystalline film (Fig. 4b, curve *1*) represents a typical emission of the Tb^{3+} ions due to the 4*f*–4*f* transitions from the excited $^5D_4$ level to the ^7F_j (j = 6–4) levels of the ground state with the most intense bands with maxima at 492, 544, 584, 625, and 667 nm. The characteristic feature of the luminescence of the Tb^{3+} cations in the $TbAlO_3$ single-crystalline film is a rather high intensity of their emission even in the range of room temperature [23].

The cathodoluminescence spectrum of the $TbAlO_3$: Ce single-crystalline film at a temperature of 80 K is shown in Fig. 4b (curve *2*). The luminescence band with a maximum at approximately 346 nm corresponds to the 5*d* ($^2T_{2g}$) $\longrightarrow$ $4f^1$ ($^2F_{5/2, 7/2}$) radiative transitions in the Ce^{3+} ions. It should be noted that the luminescence of the Ce^{3+} ions in the $TbAlO_3$ single-crystalline films is quenched to a considerable extent in the range of room temperature. One of the factors responsible for this circumstance is a substantial overlapping of the emission band of the Ce^{3+} ions (Fig. 4b, curve *2*) with the absorption bands of the Tb^{3+} cations that are attributed to the transitions $^7F_6 \longrightarrow {}^5L_9$, $^5G_4$, $^5L_{10}$, and $^5G_6 + {}^5D_3$ (Fig. 3c, curve *2*). The spectral positions of these bands correspond to the range of the maximum of the emission band of the Ce^{3+} ions. This results in the radiative transitions in the Tb^{3+} cations from the $^5D_4$ level. The conditions for the excitation energy transfer $Ce^{3+} \longrightarrow Tb^{3+}$ were considered in more detail in a separate work.

4. CONCLUSIONS

Thus, in this work, it has been demonstrated for the first time that doped and undoped single-crystalline films $RAlO_3$ (R = Y, Lu, Tb) can be grown by liquid-phase epitaxy on $YAlO_3$ single-crystalline substrates at a considerable mismatch (up to 1.44%) between the lattice constants of the single-crystalline film and the substrate. The most probable mechanism of crystallization of these single-crystalline films is the formation of transition layers between the single-crystalline film and the substrate, which leads to a gradual decrease in the difference between their lattice constants.

Taking into account that qualitative single-crystalline films $RAlO_3$ (R = Y, Lu, Tb) crystallize on the $YAlO_3$ single-crystalline substrates, the inference was made that the limiting values of the mismatch between the lattice constants of the single-crystalline films and the substrate at which the single-crystalline films of

these perovskites can be grown are as follows: $-1.44\% < \Delta a < +0.96\%$, $-0.03\% < \Delta b < +0.48\%$, and $-0.74\% < \Delta c < +0.71\%$.

The absorption, luminescence, and scintillation properties of the Ce^{3+}-doped single-crystalline films $RAlO_3$ (R = Y, Lu, Y–Lu, Tb), as well as the $TbAlO_3$ single-crystalline films grown from melt solutions based on $PbO–B_2O_3$ fluxes, were investigated. It was revealed that, on the whole, the single-crystalline films exhibit optical properties similar to the properties of the corresponding bulk single crystals. The specific features of the luminescence and scintillation properties of the single-crystalline films (in particular, a lower (10–30%) radioluminescence light yield for the (Y–Lu)AlO_3 : Ce single-crystalline films as compared to their bulk single-crystalline analogs) are associated with the doping of single-crystalline films by Pb^{2+} ions (as flux components) and their quenching effect on the Ce^{3+} luminescence. The above disadvantage of the phosphors based on the single-crystalline films can be eliminated using lead-free fluxes, specifically, a flux based on the $BaF_2–BaCO_3–B_2O_3$ system. However, compared to their bulk analogs, the (Y–Lu)AlO_3 : Ce single-crystalline films are characterized by faster decay kinetics of Ce^{3+} luminescence upon high-energy excitation due to the absence of antisite defects and the lower concentration of vacancy-type defects in these films.

ACKNOWLEDGMENTS

This study was supported in part by the Deutsche Forschungsgemeinschaft (project no. Wi-393/24-1).

REFERENCES

1. A. M. Balbashov and A. Ya. Chervonenkis, *Magnetic Materials for Microelectronics* (Énergiya, Moscow, 1979) [in Russian].
2. J. P. van der Ziel, W. A. Bonner, L. Kopf, and L. G. van Uitert, Phys. Lett. A **42**, 105 (1972).
3. M. Nakieska, J. Kosko, J. Sarnecki, M. Malinowski, and R. Piramidiwicz, Opt. Mater. **30**, 759 (2008).
4. J. M. Robertson and M. V. van Tol, Thin Solid Films **114** (1–2), 221 (1984).
5. Z. D. Hrytskiv, Y. Zorenko, V. Gorbenko, A. D. Pedan, and W. I. Shkliarskyi, Radiat. Meas. **42** (4–5), 933 (2007).
6. Y. Zorenko, V. Gorbenko, E. Mihokova, M. Niki, K. Nejezchleb, A. Vedda, V. Kolobanov, and D. Spassky, Radiat. Meas. **42** (4–5), 521 (2007).
7. P. Prusa, T. Cechak, J. A. Mares, M. Nikl, Yu. V. Zorenko, V. I. Gorbenko, J. Tous, and K. Blazek, Appl. Phys. Lett. **92** (1), 1 (2008).
8. Yu. Zorenko, V. Gorbenko, I. Konstankevych, B. Grinev, and M. Globus, Nucl. Instrum. Methods Phys. Res., Sect. A **486**, 309 (2002).
9. T. Martin and A. Koch, J. Synchrotron Radiat. **13**, 180 (2006).
10. Yu. Zorenko, V. Gorbenko, I. Konstankevych, A. Voloshinovskii, G. Stryganyuk, V. Mikhailin, V. Kolobanov, and D. Spassky, J. Lumin. **114** (4), 85 (2005).
11. Y. Zorenko, V. Gorbenko, T. Voznyak, M. Batentschuk, A. Osvet, and A. Winnacker, J. Lumin. **128** (4), 652 (2008).
12. Y. Zorenko and V. Gorbenko, Radiat. Meas. **42** (4–5), 907 (2007).
13. M. E. Globus and B. V. Grinev, *Inorganic Scintillators: New and Conventional Materials* (Akta, Khar'kov, 2000) [in Russian].
14. M. Nikl, J. Pejchal, A. Yoshikawa, T. Fukuda, A. Krasnikov, A. Vedda, and K. Nejezchleb, in *Proceedings of the Eighth International Conference on Inorganic Scintillators and Their Use in [!]Scientific and Industrial Applications (SCINT-2005), Alushta, Ukraine, 2005* (Kharkov, 2006), p. 89.
15. Yu. Zorenko, V. Gorbenko, I. Konstankevych, M. Pashkovsky, M. Globus, B. Grinyov, V. Tarasov, P. Dorenbos, C. W. E. van Eijk, and Edgar van Loef, in *Proceedings of the Fifth International Conference on Inorganic Scintillators and Their Applications, Moscow, Russia, 1999* (M. V. Lomonosov Moscow State University, Moscow, 2000), p. 476.
16. B. Ferrand, B. Chambaz, and M. Couchaud, Opt. Mater. **11**, 101 (1999).
17. Yu. Zorenko, V. Gorbenko, I. Konstankevych, T. Voznjak, V. Savchyn, M. Nikl, J. A. Mares, K. Blazelk, K. Nejezchleb, B. Grinyov, V. Mikhailin, V. Kolobanov, D. Spassky, and B. Grinyov, in *Proceedings of the Eighth International Conference on Inorganic Scintillators and Their Use in [!]Scientific and Industrial Applications (SCINT-2005), Alushta, Ukraine, 2005* (Kharkov, 2006), p. 211.
18. R. V. Telesnin, A. M. Zyuzin, V. V. Randoshkin, and Yu. V. Starostin, Fiz. Tverd. Tela (Leningrad) **24** (4), 1166 (1982) [Sov. Phys. Solid State **24** (4), 658 (1982)].
19. http://abulafia.mt.ic.ac.uk/shannon/radius.php.
20. M. Nikl, V. V. Laguta, and A. Vedda, Phys. Status Solidi B **245** (9), 1701 (2008).
21. D. K. Sardar, K. L. Nash, R. M. Yow, J. B. Gruber, U. V. Valiev, and E. P. Kokanyan, J. Appl. Phys. **100**, 083 108 (2006).
22. P. Dorenbos, J. Lumin. **91**, 91 (2000).
23. M. Sekita, Y. Miyazawa, S. Morita, H. Sekiwa, and Y. Sato, Appl. Phys. Lett. **65**, 2380 (1994).

Translated by O. Borovik-Romanova